Journal of Physics D:
Applied Physics

PAPER

Infrared spectroscopy characterization of 3C–SiC epitaxial layers on silicon

To cite this article: Olivier Pluchery and Jean-Marc Costantini 2012 *J. Phys. D: Appl. Phys.* **45** 495101

J. Phys. D: Appl. Phys. **45** (2012) 495101 (7pp) doi:10.1088/0022-3727/45/49/495101

Infrared spectroscopy characterization of 3C–SiC epitaxial layers on silicon

Olivier Pluchery[1] **and Jean-Marc Costantini**[2]

[1] Institut des NanoSciences de Paris, Université Pierre et Marie Curie UPMC-CNRS, 4 place Jussieu, 75005 Paris, France
[2] CEA, DEN, SRMA, 91191 GIF SUR YVETTE Cedex, France

Received 7 May 2012, in final form 9 October 2012
Published 9 November 2012
Online at stacks.iop.org/JPhysD/45/495101

Abstract
We have measured the transmission Fourier transform infrared spectra of cubic silicon carbide (3C–SiC polytype) epitaxial layer with a 20 μm thickness on a 200 μm thick silicon substrate. Spectra were recorded in the 400–4000 cm^{-1} wavenumber range. A novel approach of IR spectra computations based on the recursion capability of the C programming language is presented on the basis of polarized light propagation in layered media using generalized Fresnel's equations. The complex refractive indices are the only input parameters. A remarkable agreement is found between all of the experimental SiC and Si spectral features and the calculated spectra. A comprehensive assignment of (i) the two fundamental transverse optical (TO) (790 cm^{-1}) and longitudinal optical (LO) (970 cm^{-1}) phonon modes of 3C–SiC, (ii) with their overtones (1522–1627 cm^{-1}) and (iii) the two-phonon optical-acoustical summation bands (1311–1409 cm^{-1}) is achieved on the basis of available literature data. This approach allows sorting out the respective contributions of the Si substrate and SiC upper layer. Such calculations can be applied to any medium, provided that the complex refractive index data are known.

(Some figures may appear in colour only in the online journal)

1. Introduction

Silicon carbide (SiC) is a refractory material that can be used in harsh environments, such as in nuclear and space applications, in which materials are submitted to radiation damage, and sometimes high temperatures. Moreover, high-temperature ion implantation for doping of this wide band-gap semiconductor with a high breakdown voltage has also been devised for microelectronics applications. Evolution of crystalline quality is a key issue for electronic transport in this material. Therefore, Raman scattering has long been widely used to characterize the common SiC polytypes (3C, 4H, 6H, 12R) [1–4]. Raman scattering proved to be a powerful tool for investigating damage induced to silicon carbide by radiation and this technique is able to monitor changes in the vibration modes of hexagonal (4H/6H) SiC, and hence the structure modifications like amorphization induced by heavy-ion irradiations [5, 6]. A tunable sample depth from about 1 to 5 μm is probed with Raman spectroscopy using the confocal geometry. However, the self-absorption of the incident and scattered argon laser light (at 514.5 nm, i.e. for a photon energy ~2.4 eV) may bias the interpretation of Raman peak intensity evolution with damage, because of band-gap narrowing (from $E_g \sim 3.2$ eV for 6H–SiC to ~1 eV for the amorphous phase) [6]. Other techniques, such as Rutherford backscattering channeling spectrometry [7, 8] and x-ray diffraction [9], have provided valuable data on the lattice disorder in 6H– and 3C–SiC single crystals at large scale. However, there is a need for characterization with different experimental techniques of silicon carbide with a variable degree of lattice disorder at shorter scales, obtained upon non-equilibrium processes such as ion irradiation, in order to compare with the simulations at the atomic scale by molecular dynamics [10]. Moreover, it is necessary to probe the whole damaged depth, including the ion end-of-range region where the nuclear-collision damage peak is found.

It is well known that infrared absorption spectroscopy is a complementary tool for material characterization, since it gives access to IR-active vibration modes which are different from the Raman modes. Only scarce Fourier transform infrared (FTIR) data are actually available in the literature on the various SiC polytypes and were recorded

using either attenuated total reflection (ATR) configuration for thick samples [11], transmission mode for thin samples or films [11–16], or reflection geometry [17, 18]. ATR or reflection configurations probe only the topmost surface of the samples and were the most common measurements [19, 20]. Only few IR data have been obtained in the transmission mode on the thin amorphous SiC layers produced by layer deposition with thermal quenching [21–24] or by ion irradiations of 3C or 6H polytypes [25–29] and on the nanocrystalline materials resulting from subsequent thermal annealing. The interpretation of FTIR spectra is based on the detailed assignment of the detected vibrational features. However, assignments of IR bands were proposed mostly back in the 1960s, with very few recent contributions [30] and to our knowledge, no complete assignment is available for SiC.

In this paper, we present a precise FTIR characterization of 3C–SiC epitaxial layers on a silicon substrate which we have restricted to the transmission FTIR absorption spectra and that will be useful for material characterization. The transmission geometry is well adapted since this sample is mostly transparent in the middle infrared range being investigated (400–4000 cm^{-1}). Our approach is based on the detailed comparison between experimental FTIR spectral analysis and simulations using a novel computer code. The code is an analytic calculation based on the generalized Fresnel's equations using the complex refractive index as input data. A quantitative agreement is found between the experimental and simulated FTIR spectra for both the SiC epilayer and silicon substrate. This approach allows a comprehensive assignment of all the detected peaks.

2. Experimental

We have used a standard (1 0 0)-oriented n-type (nitrogen-doped) 3C–SiC epitaxial layer with 20 μm thickness ($N_\mathrm{d} - N_\mathrm{a} \sim 10^{16}\,\mathrm{cm}^{-3}$) on a p-type (boron-doped) silicon substrate with 200 μm thickness, provided by the NOVASiC Company (Le Bourget, France). Heteroepitaxial growth was carried out in a horizontal low-pressure, resistively heated, hot wall chemical-vapour deposition reactor. Measurements have also been made on a reference n-type Si single crystal with 500 μm thickness. Non-polarized transmission FTIR spectra have been measured at room temperature with a Bruker Tensor-27 spectrometer in the 400–4000 cm^{-1} wavenumber range with a spectral resolution of 4 cm^{-1}. In order to minimize the interference fringes, spectra were recorded near Brewster's incidence angle ($\theta_\mathrm{B} = \arctan n = 68°$) with an IR refractive index $n = 2.55$ for SiC [31]. Optimal results were obtained for an incidence angle $\theta = 72°$. Similar measurements were performed at $\theta = 72°$ for the Si substrate with $n = 3.42$ [32] and $\theta_\mathrm{B} = 73.7°$. A similar procedure was used for measurements of FTIR spectra of amorphous silicon nitride films [33], alumina film [34] or other oxide thin films [35, 36].

3. Computation of FTIR spectra

From an optical point of view, thin films can be modelled as series of layers of infinite lateral extension, each one being characterized by an optical index and its thickness. The optical beam is correctly described by a plane wave of circular frequency ω and of wavelength in vacuum λ_0. In principle, the Maxwell equations and the boundary conditions are sufficient to completely determine the behaviour of the light beam through any combination of thin films and the description of this problem is accessible to undergraduate students. However, its resolution is not an easy task and this problem often requires a numerical resolution. Since the first algorithms (see for example the recursion approach from Rouard in 1937 [37] or the matrix approach developed by Abeles in 1948 [38]), many algorithms have been developed and the power of computing makes now an accurate solution accessible to desktop personal computers. We briefly review the problem and describe the approach we have developed to calculate IR spectra using as only input parameters the optical indices and the geometrical data (layer thicknesses, polarization state and incidence angles).

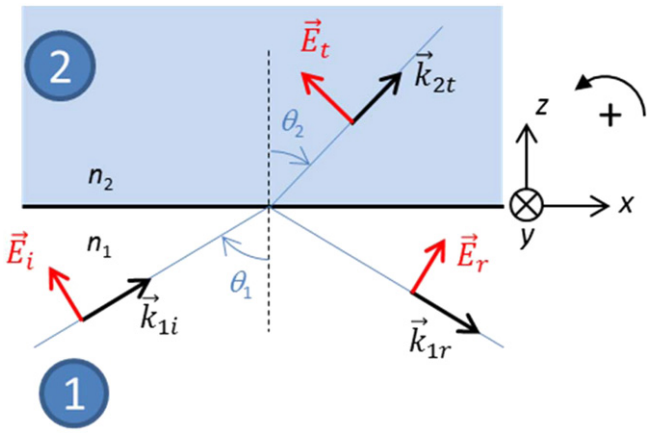

Figure 1. Interface between medium 1 and medium 2 characterized by their indices n_1 and n_2. The incidents, reflected and transmitted electric fields are drawn in the case of a p-polarized incident field. This sketch defines all the sign conventions used in the formulae.

3.1. Generalized Fresnel formulae

Let us consider a linearly polarized optical beam, impinging on the first layer of a multilayered system with an incident angle θ_1. Its polarization state can be expressed as a combination of the two polarization states p and s, these two letters standing for *parallel* and perpendicular (*senkrecht* in German) to the plane of incidence. We consider only isotropic medium which means that the polarization is not modified when the beam is going through the medium. Notations are explained in figure 1: z-axis is chosen normal to the interface so that the incident wave travels in the positive z direction; the x-axis is taken in the plane of incidence so that the wavevectors have only x and z components. In the following, we give some details in the case of p-polarization and the corresponding quantities are indicated with p as superscript. The incident electric field is as follows:

$$\vec{E}_\mathrm{i}^\mathrm{p}(\vec{r}, t) = \vec{E}_{\mathrm{i}0}^\mathrm{p} \mathrm{e}^{\mathrm{i}(\vec{k}_\mathrm{i}.\vec{r} - \omega t)}. \quad (1)$$

At the interface between medium 1 and medium 2, a reflected beam and a transmitted beam are generated and

they are characterized by their wavevectors $\vec{k}_r$ and $\vec{k}_t$ and their amplitudes $\vec{E}^p_{r0}$ and E^p_{t0}. For non-absorbing media, the wavevector is expressed as follows:

$$\vec{k} = \frac{2\pi}{\lambda_0} n\vec{u}, \tag{2}$$

where λ_0 is the wavelength in vacuum, n is the refractive index of the medium and $\vec{u}$ is the propagation direction. If the medium is absorbing, the propagation can be described in a similar way by replacing n with the complex index $\tilde{n} = n + ik$ [39][3].

The continuity of the component of the electric field parallel to the interface leads to the following relations:

$$E^p_{i0}\cos\theta_1 + E^p_{r0}\cos\theta_1 = -E^p_{t0}\cos\theta_2, \tag{3}$$

$$k_{ix} = k_{rx} = k_{tx}. \tag{4}$$

Equation (4) means that the components of all the wavevectors parallel to the interface should be equal to one another and it results from the fact that the argument in the exponential of each of the three waves should be synchronized at the interface when position is exploring the interface ($\vec{r} = x\vec{u}_x + y\vec{u}_y$). Snell's law is derived from equation (4), when the media are non-absorbing, given that $k_x = (2\pi/\lambda_0)n\sin\theta$. The continuity for the magnetic excitation $\vec{H}$ at the interface leads to an equation similar to (3):

$$k_i E^p_{i0} + k_r E^p_{r0} = k_t E^p_{t0}. \tag{5}$$

By eliminating E^p_{t0} between equations (3) and (5) one can derive the reflection coefficient in amplitude at the interface between media 1 and 2, $r^P_{12} = E^p_{r0}/E^p_{i0}$ given by

$$r^P_{12} = \frac{n_2\cos\theta_1 - n_1\cos\theta_2}{n_2\cos\theta_1 + n_1\cos\theta_2}. \tag{6}$$

This is one of the four well-known Fresnel's formulae [39].

However, if one wants to use this equation for absorbing media, a first difficulty appears: in this case, $\tilde{n}_2$ is complex and the angle θ_2 would also be complex which is inappropriate. Therefore, angles should not be used for treating absorbing media and the projections expressed in equation (3) should be replaced by a generalized expression. This is achieved by generalizing equation (4): for a system of stacked layers, at layer number l, an invariant is defined as the complex quantity $\tilde{n}_l q_l$ defined by

$$\tilde{n}_l q_l = n_1\sin\theta_1 \qquad (\text{for any } l > 1). \tag{7}$$

The projection of the wave vector normal to the interface (analog to $\cos\theta_l$) is generalized by the expressions $\sqrt{1-q_l^2}$. Therefore the Fresnel formulae for the reflected beams in polarization p and s at the interface between 1 and 2, is transformed into

$$r^P_{12} = \frac{\sqrt{1-q_1^2} - \frac{\tilde{n}_1}{\tilde{n}_2}\sqrt{1-(\frac{\tilde{n}_1}{\tilde{n}_2}q_1)^2}}{\sqrt{1-q_1^2} + \frac{\tilde{n}_1}{\tilde{n}_2}\sqrt{1-\left(\frac{\tilde{n}_1}{\tilde{n}_2}q_1\right)^2}}, \tag{8}$$

[3] If the phase of the plane wave is defined by $\omega t - k.r$ (see equation (1)), the complex index should be expressed by $\tilde{n} = n + ik$ as some authors do (Born & Wolf).

$$r^s_{12} = \frac{\frac{\tilde{n}_1}{\tilde{n}_2}\sqrt{1-q^2} - \sqrt{1-\left(\frac{\tilde{n}_1}{\tilde{n}_2}q\right)^2}}{\frac{\tilde{n}_1}{\tilde{n}_2}\sqrt{1-q^2} - \sqrt{1-\left(\frac{\tilde{n}_1}{\tilde{n}_2}q\right)^2}} \tag{9}$$

and the transmission coefficients are given by

$$t^P_{12} = \frac{2\sqrt{1-q_1^2}}{\frac{\tilde{n}_2}{\tilde{n}_1}\sqrt{1-q_1^2} + \sqrt{1-\left(\frac{\tilde{n}_1}{\tilde{n}_2}q_1\right)^2}}, \tag{10}$$

$$t^s_{12} = \frac{2\sqrt{1-q_1^2}}{\sqrt{1-q_1^2} + \frac{\tilde{n}_2}{\tilde{n}_1}\sqrt{1-\left(\frac{\tilde{n}_1}{\tilde{n}_2}q_1\right)^2}}. \tag{11}$$

These formulae can be used for interfaces between any kind of layers (non-absorbing or absorbing).

3.2. Reflected and transmitted beams in a three-layer system

Let us now consider a system made of three layers, of indices $\tilde{n}_1$, $\tilde{n}_2$ and $\tilde{n}_3$. Medium 2 has a thickness d_2 and the two other ones are considered as semi-infinite in the z direction. The reflection ($\mathcal{R}_2$) and transmission ($\mathcal{T}_2$) coefficients of this thin film can be calculated as a function of Fresnel's coefficients of each interface (figure 2(a)). The calculation takes into account the multiple reflections within layer 2 (interferences patterns) and yields the following results:

$$\mathcal{R}_2 = r_{12} + \frac{t_{12}\cdot t_{21}\cdot r_{23}\cdot e^{2i\delta_2}}{1 + r_{12}\cdot r_{23}\cdot e^{2i\delta_2}}, \tag{12}$$

$$\mathcal{T}_2 = \frac{t_{12}\cdot t_{23}\cdot e^{i\delta_2}}{1 + r_{12}\cdot r_{23}\cdot e^{2i\delta_2}}, \tag{13}$$

δ_2 is the phase factor given by $\delta_2 = (2\pi/\lambda_0)\tilde{n}_2 d_2\sqrt{1-q_2^2}$. The superscript p and s of Fresnel's coefficients are not indicated since the formulae are identical for both polarizations.

3.3. Recursion method to treat numerically any number of layers

The formulae given above are robust enough to be applied to any type of layers characterized by their complex indices. They are rather simple and make feasible numerical calculations of the reflection and transmission coefficients through any numbers of layers using the recursion property, which is well known in computer science. The recursion method was proposed in 1934 by Rouard [37], explained by Heavens in 1955 [40], and was used to derive analytical expressions of the reflection and transmission in specific cases. However, as Heavens himself stated: 'the case of systems of absorbing films at non-normal incidence, where the angles involved in the expressions for the Fresnel coefficients are also complex, is depressing indeed' [40]. Actually, most authors have usually opted for the matrix method pioneered by Abeles [38] and

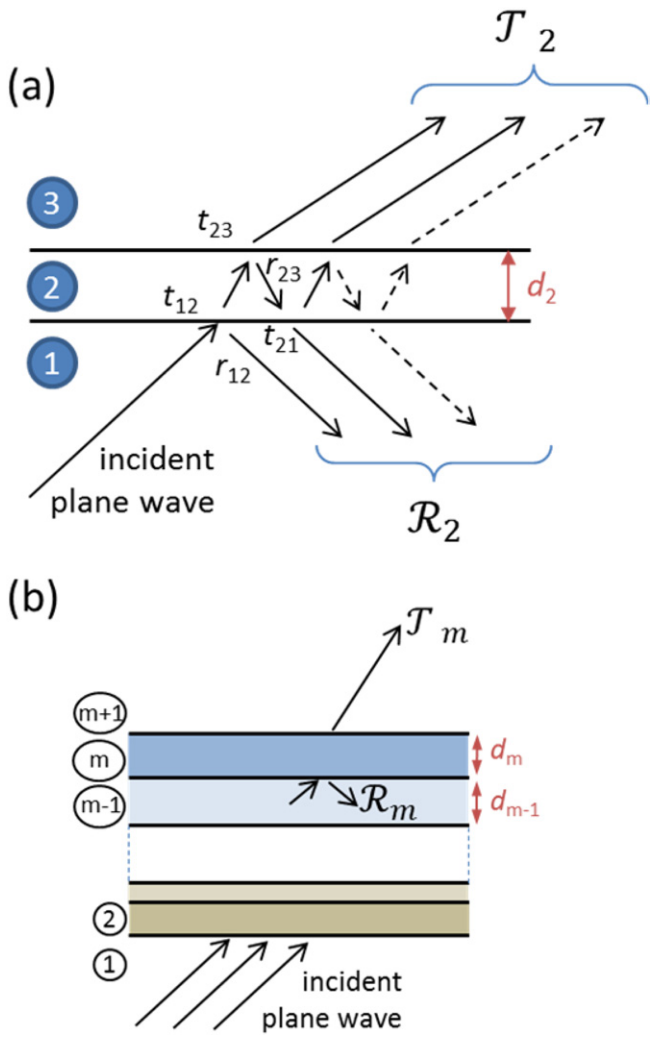

Figure 2. The case of a plane wave impinging on a single layer is described by a three-layer model. The transmission and reflection coefficients T_2 and R_2 can be calculated as a function of Fresnel's coefficients indicated on the figure and take into account the multiple reflections occurring inside medium 2 (a), recursion approach for calculating the transmission and reflection across a system made of $m-1$ layers. The transmitted field into medium m+1 is given by the coefficient T_m calculated by a 3-layer model where the incident field results from the transmission through the $m-2$ previous layers (coefficient T_{m-1}) (b). This step-by-step calculation is part of the recursion capability of most modern programming languages.

the recursion approach promoted by Rouard [37] seems to have been mostly overlooked, except in a few cases (see for example [41, 42]). However, although this method is not very efficient for analytical derivations, it is well suited to numerical calculations. This recursion approach devised by Rouard in 1934 is now implemented as a built-in property in most modern computer codes. It consists in a function that needs to call itself to proceed in the calculation until break conditions is reached. It was initiated by languages such as Algol and LISP in the early 1970s.

In our case, if we consider the case of a series of m+1 media of indices $\tilde{n}_l$, the calculation of the transmitted beam through this set of $m-1$ layers can be expressed as a function of the same problem for the media $1, \ldots, m$. According to equation (13) the transmitted amplitude $\mathcal{T}_m$ through this system is given

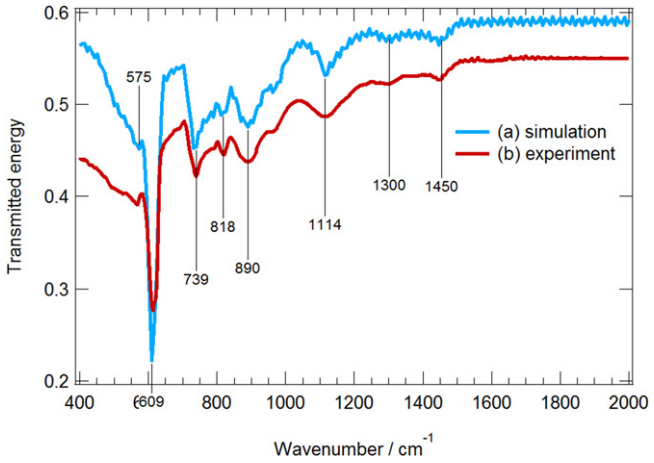

Figure 3. Simulated (light blue curve) (a) and measured (red curve) (b) transmission spectra through a 500 μm thick weakly-doped silicon sample for an incidence angle $\theta = 72^\circ$ near Brewster's angle.

by [40]

$$\mathcal{T}_m = \frac{t_{m-1,m} \cdot t_{m,m+1} \cdot e^{i\delta_m}}{1 + r_{m-1,m} \cdot r_{m,m+1} \cdot e^{2i\delta_m}}.$$

In this expression, $t_{m,m+1}$ and $r_{m,m+1}$ are Fresnel's coefficient of the last interface between medium m and medium $m+1$ that can be straightforwardly calculated with equations (10) or (11): $t_{m-1,m}$ is the transmitted amplitude through the m previous media and is given by $\mathcal{T}_{m-1}$. Similarly one has $r_{m-1,m} = \mathcal{R}_{m-1}$. This means that the calculation calls itself but with a decreasing index m. This recursion calculation proceeds until interface 1–2 is reached where reflection/transmission coefficients are given by Fresnel's formulae. This calculation can be carried out for each wavelength. If the complex indices of each layer are precisely known the reflectivity and transmission spectra can be computed accurately provided the beam energy is calculated with the expressions:

Reflected energy: $R = |\mathcal{R}_m|^2$,
Transmitted energy: $T = \frac{\cos\theta_m}{\cos\theta_1}|\mathcal{T}_m|^2$.

This code has been implemented in C within the Igor Pro software (from Wavemetrics®). All the calculated spectra presented in this study are constituted with 500 sampling points in the wavelength range of interest and up to four layers. The calculations are made with an ordinary desktop pc and take less than 1 s.

3.4. Test of computer code on a reference silicon sample

In order to test our approach, we have carried out simulations of the spectra using the above-mentioned computer code devised to calculate the IR absorption of multilayered solids. For this purpose, the generalized Fresnel's laws of reflection were used for a variable incidence angle (θ), as explained above. As such, it is feasible to calculate the propagation of a p-polarized wave (at $\theta = \theta_B$) in an air/Si/air sample, provided that the data of the real (n) and imaginary (k) part of the refractive index of these materials are available. For this, Palik's compilation of experimental refractive index data [32] was used to obtain the absorbance of these samples in the IR range. In order

Table 1. IR absorption peaks of the Si reference sample with their possible assignments to vibration modes (figure 3).

ν (cm^{-1})	575	609	739	818	890	1114	1300	1450
Intensity	Weak	Strong	Medium	Weak	Medium	Strong	Weak	Weak
Mode	Si (LO+TA)	Si (TO+TA)	Si (LO+LA)	Si (TO+LA)	Si (TO+LO)	Si–O (stretching)	Si (2TO+LA)	Si (3TO)

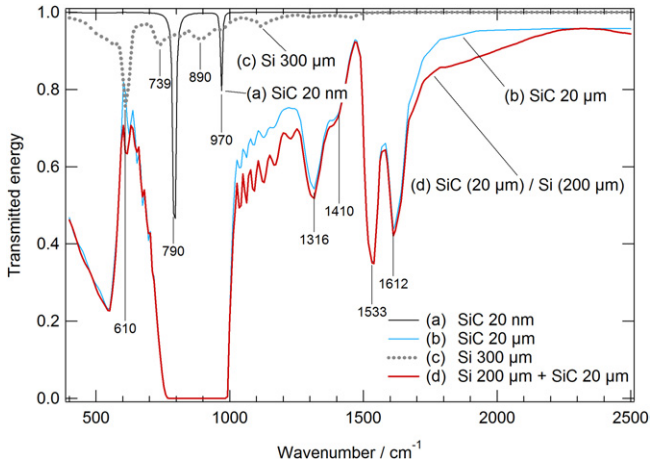

Figure 4. Simulations of transmission spectra with the algorithm depicted in this paper. Four cases are presented: an ultrathin SiC layer of 20 nm (*a*) (grey solid curve), a SiC thin film of 20 μm thickness (*b*) (blue solid curve), a silicon wafer (undoped silicon) of 300 μm thickness (*c*) (grey dotted curve), and a more realistic system with a 20 μm SiC layer on top of a 200 μm silicon substrate (*d*) (red solid curve). In all cases the thin films are placed in a medium of optical index $n = 1$ (vacuum or air). Simulations were carried out for an incidence angle $\theta = 68^\circ$ (near Brewster's angle) and for *p*-polarized light. The only input parameter is the complex optical indices, taken from Palik's handbook of optical data [32].

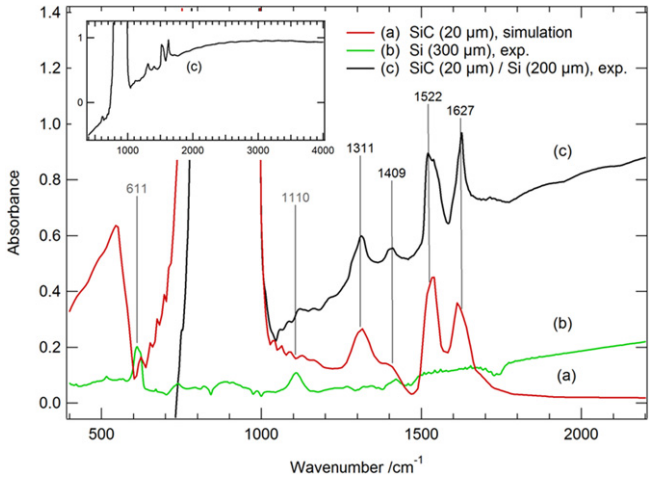

Figure 5. Experimental FTIR transmission spectra compared with simulations: 20 μm thick SiC thin film calculated according to the algorithm presented in the text (shown in figure 4) and transformed into absorbance unit to match the experimental data (*a*) (red curve), experimental absorbance of a 300 μm undoped silicon sample for an incidence angle $\theta = 72^\circ$ (*b*) (green curve), absorbance of the sample of interest (20 μm SiC grown on a 200 μm Si substrate) for an incidence angle $\theta = 72^\circ$ (*c*) (black curve). The experimental absorbance is processed using a reference spectrum obtained with the empty sample compartment of the spectrometer (normalization by the spectral characteristics of the lamp and the detector). The inset shows the whole recorded spectrum of SiC/Si (*c*).

to carry out a detailed comparison between computed and measured spectra, the experimental spectrum is recorded with a high purity float zone (FZ) silicon sample. Moreover, it is a double side polished, 500 μm thick and low doped (20 Ω cm, phosphorous-doped) sample. This last characteristic prevents the sample from absorbing IR light at wavenumbers higher than 2000 cm^{-1}.

The computed and experimental spectra are displayed in the wavenumber range from 400 to 2000 cm^{-1} (figure 3). No specific absorption features are seen beyond 2000 cm^{-1}. The two spectra are almost identical and the seven absorption bands of Si are remarkably reproduced. The simulation spectrum displays slight interference patterns that are barely visible in the experimental one because of the smearing out due to our experimental spectral resolution. Note that the interference patterns can also be suppressed using single side polished samples: in such a case, the roughness of the sample backside prevents multiple internal reflections. Such a method will be used in section 4 of this work. However, in this section, since our computing model is restricted to perfectly plane interfaces, we have chosen double side polished substrate for our comparisons. The seven detected peaks are due to two- and three-phonon (optical/acoustical) modes (table 1) [43, 44]. The main peak at 609 cm^{-1} can be assigned to the two-phonon (TO + TA) mode. The other six peaks at 575 cm^{-1}, 739 cm^{-1}, 818 cm^{-1}, 890 cm^{-1}, 1300 cm^{-1} and 1450 cm^{-1} can be assigned to the two-phonon (LO + TA), (LO + LA), (TO + LA), (TO + LO), and three-phonon (2TO + LA), and 3TO modes, respectively [43, 44]. Calculations also display one weak extra peak at 1114 cm^{-1} that can be assigned to the Si–O stretching mode [44, 45], due to the traces of oxygen impurities that are commonly found in Si samples [43] even in FZ samples. As is well known, no absorption peaks due to single TO and LO modes are observed in silicon which is a non-polar solid [43]. The respective peak intensities in the calculated spectra also match rather well the experimental data.

4. Application to silicon carbide

Calculations of the transmitted energy through air/SiC/air and air/SiC/Si/air samples that are of interest in this paper are displayed in figure 4. In the case of a 20 nm ultrathin SiC layer, the spectrum exhibits two strong peaks at 790 cm^{-1} and 970 cm^{-1}, assigned, respectively, to the optical (TO and LO) phonon modes of crystalline SiC. These absorption peaks dominate all the other features with an absorption efficiency of 50% approximately. The simulation of absorption through a 1000-times thicker SiC layer (figure 4) shows other peaks and of course, a total absorption of light around the two

Table 2. IR absorption peaks of the 3C–SiC/Si sample with their possible assignments to vibration modes (figure 5).

ν (cm^{-1})	611	1110	1311	1409	1522	1627
Intensity	Very weak	Very weak	Weak	Weak	Medium	Medium
Mode	Si (TO+TA)	Si–O (stretching) Si–C (TO+TA)	Si–C (TO+LA)	Si–C (LO+LA)	Si–C (2TO)	Si–C (TO+LO)

main phonon peaks mentioned above. Supplemental peaks are found at 1316, 1410, 1533 and 1612 cm^{-1} that have an absorption efficiency of roughly 50% also, pointing to vibrational modes of ~1000-times weaker oscillator strengths than the TO and LO modes. In these simulations, the absorption through a 300 μm thick silicon sample is also presented (figure 4). This sample has characteristics close to that of the silicon substrate used for growing SiC in terms of polishing, thickness doping and growing method (standard Czochralski growing method). It shows that the silicon substrate has almost no contribution in the spectral range of interest except the strongest two-phonon (TO + TA) mode at ~ 610 cm^{-1} (figure 3). As expected, a much lower absorbance than for SiC is found owing to the smaller oscillator strength for non-polar bonds.

Experimental FTIR absorption spectra are displayed in figure 5. The whole spectrum presented in the inset is calculated using a reference spectrum recorded without any sample and it shows that the absorbance gradually increases with wavenumbers up to 0.9 absorbance unit above 2000 cm^{-1}. It illustrates the IR absorption due to the free carriers of the silicon substrate. Note that simulations have been carried out with undoped samples so that the spectrum baseline remains flat. The negative absorbance displayed at low wavenumbers is an artefact due to a change in the optical path when setting up the sample and is not related to any physical effect. A huge absorption feature is found in the wavenumber range between 600 and 1000 cm^{-1} for the 3C–SiC epilayer mainly arising from the fundamental IR-active vibration modes of SiC (figures 3 and 4). Actually, it mainly corresponds to the TO and LO phonon modes of SiC [2, 3, 46], whilst the two smaller peaks at 1522 and 1627 cm^{-1} (with significant absorbances ~0.5) likely arise from the first overtones of these two modes (figure 4). Much smaller contributions (with absorbances <0.15) arise from the Si substrate at 611 cm^{-1}, corresponding to the strongest Si two-phonon (TO + TA) mode [44], and at 1114 cm^{-1}, corresponding to the Si–O stretching modes due to oxygen impurities (figure 3) [43–45], or to the two-phonon (TO + TA) mode of SiC [2, 3, 14]. The two extra peaks at 1311 and 1409 cm^{-1} can be assigned to the (TO + LA) and (LO + LA) optical-acoustical summation bands of Si–C vibration modes, respectively, like for ATR or transmission spectra of 6H–SiC showing five two-phonon combination bands in the spectral range between 1000 and 1800 cm^{-1} [2, 3, 11, 14]. Table 2 displays all these peaks with the possible assignments.

Excellent agreement of the calculated spectra with the experimental one is found for the SiC/Si epilayer showing the fundamental modes with their overtones and optical-acoustical summation bands of SiC, and two weak peaks of Si. Actually, all of the peaks found in the experimental spectra for SiC and Si, are seen in the simulated ones (tables 1 and 2). Moreover, our experimental data for SiC are in very good agreement with the calculated optical TO and LO phonon mode wavenumbers of 795 cm^{-1} and 972 cm^{-1}, respectively (for $q = 0$ at the Γ-point of the Brillouin zone), respectively [2, 3, 46], and their respective overtones at 1519.3 (2TO) and 1623.7 cm^{-1} (TO + LO) measured by Raman spectroscopy [2, 3] (table 2). Further experiments are under way to study the impact of ion-induced lattice disorder on the specific vibration modes of 3C–SiC epilayers.

5. Conclusions

A novel computer code has been devised to calculate the propagation of polarized light in condensed matter on the basis of generalized Fresnel's equations, provided the complex refractive index data are known. Computed transmission spectra of SiC/Si and Si samples are compared with the experimental FTIR spectra recorded at Brewster's angle for wavenumbers between 400 and 4000 cm^{-1}. A test of the computer code is carried out against the Si data. All of the experimental peaks are seen in the computed spectra for both materials. For SiC, these peaks are assigned to: (i) the fundamental optical (TO and LO) phonon modes and their overtones and (ii) two-phonon combination bands of the TO and LO modes with the acoustical (TA or LA) phonon modes. A remarkable agreement is found for all peak positions between computed and experimental data.

References

[1] Feldman D W, Parker J H Jr, Choyke W J and Patrick L 1968 Phonon dispersion curves by Raman scattering in SiC, polytypes 3C, 4H, 6H, 15R, and 21R *Phys. Rev.* **173** 787–93
[2] Olego D, Cardona M and Vogl P 1982 Pressure-dependence of the optical phonons and transverse effective charge in 3C–SiC *Phys. Rev.* B **25** 3878–88
[3] Olego D and Cardona M 1982 Pressure-dependence of Raman phonons of Ge and 3C–SiC *Phys. Rev.* B **25** 1151–60
[4] Nakashima S and Tahara K 1989 Raman-scattering determination of structures for SiC polytypes - quantitative-evaluation with a revised model of lattice-dynamics *Phys. Rev.* B **40** 6339–44
[5] Sorieul S, Costantini J M, Gosmain L, Thome L and Grob J J 2006 Raman spectroscopy study of heavy-ion-irradiated alpha-SiC *J. Phys.: Condens. Matter* **18** 5235–51
[6] Sorieul S, Costantini J M, Gosmain L, Calas G, Grob J J and Thome L 2006 Study of damage in ion-irradiated alpha-SiC by optical spectroscopy *J. Phys.: Condens. Matter* **18** 8493–502

[7] Kerbiriou X, Costantini J-M., Sauzay M, Sorieul S, Thome L, Jagielski J and Grob J-J 2009 Amorphization and dynamic annealing of hexagonal SiC upon heavy-ion irradiation: Effects on swelling and mechanical properties *J. Appl. Phys.* **105** 073513

[8] Jiang W, Zhang Y and Weber W J 2004 Temperature dependence of disorder accumulation and amorphization in Au-ion-irradiated 6H–SiC *Phys. Rev.* B **70** 165208

[9] Debelle A, Thome L, Dompoint D, Boulle A, Garrido F, Jagielski J and Chaussende D 2010 Characterization and modelling of the ion-irradiation induced disorder in 6H–SiC and 3C–SiC single crystals *J. Phys. D: Appl. Phys.* **43** 455408

[10] Gao F and Weber W J 2003 Atomic simulation of ion-solid interaction in ceramics *Nucl. Instrum.* B **207** 10–20

[11] Tsuchida H, Kamata I and Izumi K 1999 Infrared attenuated total reflection spectroscopy of 6H–SiC(0 0 0 1) and (000(1)over-bar) surfaces *J. Appl. Phys.* **85** 3569–75

[12] Spitzer W G, Kleinman D A and Frosch C J 1959 Infrared Properties of Cubic Silicon Carbide Films *Phys. Rev.* **113** 133–6

[13] Spitzer W G, Kleinman D and Walsh D 1959 Infrared Properties of Hexagonal Silicon Carbide *Phys. Rev.* **113** 127–32

[14] Patrick L and Choyke W J 1961 Lattice Absorption Bands in SiC *Phys. Rev.* **123** 813–5

[15] Gracin D, Desnica U and Ivanda M 1992 Microstructural properties of dc magnetron sputtered a-Si : H by IR spectroscopy *J. Non-Cryst. Solids* **149** 257–63

[16] Gracin D, Juraic K, Dubcek P, Gajovic A and Bernstorff S 2006 The nano-structural properties of hydrogenated a-Si and Si–C thin films alloys by GISAXS and vibrational spectroscopy *Appl. Surf. Sci.* **252** 5598–601

[17] Pernot J, Bluet J M, Camassel J and Di Cioccio L 2001 Infrared investigation of implantation damage and implantation damage anneling in 4H–SiC *Mater. Sci. Forum* **353–356** 385–8

[18] Camassel J, Pernot J, Wang H Y and Peyre H 2003 Modeling the infrared reflectance of n–/n+ SiC layers on top of n+ SiC substrates for epitaxy control application *Phys. Status Solidi* a **195** 38–43

[19] Hobert H, Dunken H H, Urban S, Falk F and Stafast H 2002 Laser-induced changes of silicon carbon films studied by vibrational spectroscopy *Vib. Spectrosc.* **29** 177–82

[20] Hobert H, Dunken H, Menzel R, Bachmann T and Wesch W 1997 Infrared and Raman spectroscopy of particle-beam induced damage of silicon carbide *J. Non-Cryst. Solids* **220** 187–94

[21] Rajagopalan T, Wang X, Lahlouh B, Ramkumar C, Dutta P and Gangopadhyay S 2003 Low temperature deposition of nanocrystalline silicon carbide films by plasma enhanced chemical vapor deposition and their structural and optical characterization *J. Appl. Phys.* **94** 5252–60

[22] Kerdiles S, Hairie A, Rizk R and Guedj C 2001 Vibrational-mode frequencies of substitutional carbon in $Si_{1-x}C_x$ alloys *Phys. Rev.* B **63** 205206

[23] Kerdiles S, Berthelot A, Gourbilleau F and Rizk R 2000 Low temperature deposition of nanocrystalline silicon carbide thin films *Appl. Phys. Lett.* **76** 2373–5

[24] Colder H, Rizk R, Morales M, Marie P, Vicens J and Vickridge I 2005 Influence of substrate temperature on growth of nanocrystalline silicon carbide by reactive magnetron sputtering *J. Appl. Phys.* **98** 024313

[25] Musumeci P, Calcagno L and Makhtari A 1998 Relaxation phenomena in keV-ion implanted hydrogenated amorphous silicon carbide *Mater. Sci. Eng.* A **253** 296–300

[26] Dkaki M, Calcagno L, Makthari A M and Raineri V 2001 Infrared spectroscopy and transmission electron microscopy of polycrystalline silicon carbide *Mater. Sci. Semicond. Process.* **4** 201–4

[27] Compagnini G, Foti G and Makhtari A 1998 Vibrational analysis of compositional disorder in amorphous silicon carbon alloys *Europhys. Lett.* **41** 225–30

[28] Chang W, Feng Z C, Lin J, Liu R, Wee A T S, Tone K and Zhao J H 2002 Infrared reflection investigation of ion-implanted and post-implantation-annealed epitaxially grown 6H–SiC *Sur. Interface Anal.* **33** 500–5

[29] Musumeci P, Reitano R, Calcagno L, Roccaforte F, Makhtari A and Grimaldi M G 1997 Relaxation and crystallization of amorphous silicon carbide probed by optical measurements *Phil. Mag.* B **76** 323–33

[30] Zollner S, Liu R, Konkar A, Gutt J, Wilson S R, Tiwald T I, Woollam J A and Hilfiker J N 1999 Dielectric function of polycrystalline SiC from 190 nm to 15 μm *Phys. Status Solidi* B **215** 21–5

[31] Goldberg Y U, Levinshtein M E and Rumyantsev S L 2001 *Properties of Advanced Semiconductor Materials GaN, AlN, SiC, BN, SiGe* (New York: Wiley)

[32] Lynch D W and Hunter W R 1985 *Handbook of Optical Constants* ed E D Palik (New York: Academic)

[33] Li T and Kanicki J 1998 Observation of incident angle dependent phonon absorption in hydrogenated amorphous silicon nitride thin films *Appl. Phys. Lett.* **73** 3866–8

[34] Busch B W, Pluchery O, Chabal Y J, Muller D A, Opila R L, Kwo J R and Garfunkel E 2002 Materials characterization of alternative gate dielectrics *MRS Bull.* **27** 206–11

[35] Lita B, Pluchery O, Opila R L, Chabal Y J, Bunea G, Holman J P and Bekos E J 2004 Wet chemical cleaning of plasma oxide grown on heated (0 0 1) InP surfaces *J. Vac. Sci. Technol.* B **22** 1885–92

[36] Pluchery O, Opila R L and Chabal Y J 2003 Wet chemical cleaning of InP surfaces investigated by *in situ* and ex situ infrared spectroscopy *J. Appl. Phys.* **94** 2707–15

[37] Rouard P 1937 *Ann. Phys.* **7** 291

[38] Abelès F 1948 *Ann. Phys.* **3** 504

[39] Born M and Wolf E 1999 *Principles of Optics: Electromagnetic Theory of Propagation, Interference and Diffraction of Light* 7th edn (Cambridge: Cambridge University Press)

[40] Heavens O S 1955 *Optical Properties of Thin Solid Films* (London: Butterworths Scientific Publications)

[41] Tomas M-S 2010 Recursion relations for generalized Fresnel coefficients: Casimir force in a planar cavity *Phys. Rev.* A **81** 044104

[42] Crawford O H 1988 Radiation from oscillating dipoles embedded in a layered system *J. Chem. Phys.* **89** 6017–27

[43] Seeger K 2004 Optical absorption and reflection *Semiconductor Physics: an Introduction* (Berlin: Springer) chapter 11

[44] Lau W S 1999 *Infrared Characterization for Microelectronics* (Singapore: World Scientific)

[45] Tsu D V, Lucovsky G and Mantini M J 1986 Local atomic-structure in thin-films of silicon-nitride and silicon diimide produced by remote plasma-enhanced chemical-vapor deposition *Phys. Rev.* B **33** 7069–76

[46] Karch K, Pavone P, Windl W, Schutt O and Strauch D 1994 Ab-Initio calculation of structural and lattice-dynamical properties of silicon-carbide *Phys. Rev.* B **50** 17054–63